
Article:
Hanson, BS orcid.org/0000-0002-6079-4506, Iida, S, Read, DJ et al. (4 more authors) (2020) Continuum Mechanical Parameterisation of Cytoplasmic Dynein from Atomistic Simulation. Methods. ISSN 1046-2023

https://doi.org/10.1016/j.ymeth.2020.01.021

Continuum Mechanical Parameterisation of Cytoplasmic Dynein from Atomistic Simulation

Benjamin S. Hanson[1], Shinji Iida[2], Daniel J. Read[3], Oliver G. Harlen[3], Genji Kurisu[2], Haruki Nakamura[2], Sarah A. Harris[14]

[1] School of Physics & Astronomy, University of Leeds, Leeds, UK, LS2 9JT
[2] Institute for Protein Research, Osaka University, 3-2 Yamadoaka, Suita, Osaka 565-0871, Japan
[3] School of Mathematics, University of Leeds, Leeds, UK, LS2 9JT
[4] Astbury Centre for Structural Molecular Biology, University of Leeds, Leeds, UK, LS2 9JT

Corresponding Author: Sarah A. Harris (s.a.harris@leeds.ac.uk)

Highlights

- Analysis of all-atom MD simulations of cytoplasmic dynein show that the majority of conformational space is explored via angular fluctuations in the stalk
- The observed dynamics of this molecule can be well represented at a coarse-grained level with FFEA, an inhomogeneous, linear viscoelastic continuum model
- Continuum parameterisation of the motor captures the higher flexibility of the ATP bound model relative to its ADP bound counterpart.

Keywords

Dynein, Molecular Dynamics, Fluctuating Finite Element, Analysis, Multiscale Simulation, Hierarchical Biomechanics, Principal Component Analysis

Abbreviations

Abbreviations defined in footnote[1].

[1] PCA – Principal Component Analysis, MD – Molecular Dynamics, FFEA – Fluctuating Finite Element Analysis, ADP – Adenosine Diphosphate, ATP – Adenosine Triphosphate, MT – Microtubule, MTBD – Microtubule binding domain

Abstract

Cytoplasmic dynein is responsible for intra-cellular transport in eukaryotic cells. Using Fluctuating Finite Element Analysis (FFEA), a novel algorithm that represents proteins as continuum viscoelastic solids subject to thermal noise, we are building computational tools to study the mechanics of these molecular machines. Here we present a methodology for obtaining the material parameters required to represent the flexibility of cytoplasmic dynein within FFEA from atomistic molecular dynamics (MD) simulations, and show this continuum representation is sufficient to capture the principal dynamic properties of the motor.

1. Introduction

The dynamics of biological macromolecules are essential to their function. All biomolecules continuously change shape due to thermal fluctuations. In molecular motors, larger conformational changes are also driven by active processes arising from directed work. Cytoplasmic dynein is a molecular motor responsible for transporting cargo throughout the microtubule network within cells. Recent optical tweezer experiments have shown that the expected maximum velocity of a cytoplasmic dynein dimer is 387 nm/s, or approximately 24 steps/s with the observed 16nm steps [1]. This implies a minimum characteristic timescale for the dynein force-generating mechanism of approximately 41ms. Atomistic molecular dynamics (MD) simulations have been used to explore the dynamics of the two conformational states of the dynein monomer over timescales of 200ns [2]. These MD simulations are extremely computationally intensive due to the large size of the motor and so, while they can explore dynamics due to the thermal fluctuations of biomolecules, the timescales associated with active processes, such as the stepping of the dynein motor, lie well outside of this regime. To account for this, we have devised a multi-scale simulation scheme that uses atomistic simulations to parameterise a highly coarse-grained continuum model known as Fluctuating Finite Element Analysis (FFEA). We aim to use this method to ultimately provide a route to multi-scale modelling of molecular machines capable of exploring the mechanical mechanism of the motor. Details of how to obtain the FFEA software are provided as Supplementary Information (S1).

Figure 1 shows a schematic representation of the dynein motor. The motor domain, responsible for the ATP hydrolysis required for directed motion, is a hexameric AAA+ ring. This domain is separated from the microtubule (MT) binding domain (MTBD) by a coiled-coil stalk domain approximately 12nm in length [3]. The ATP hydrolysis necessary for the powerstroke occurs in the motor domain, which is a hexameric AAA ring [4]. The force generated by the motor is propagated to the cargo via the linker, which protrudes from the AAA1 domain and extends across the motor.

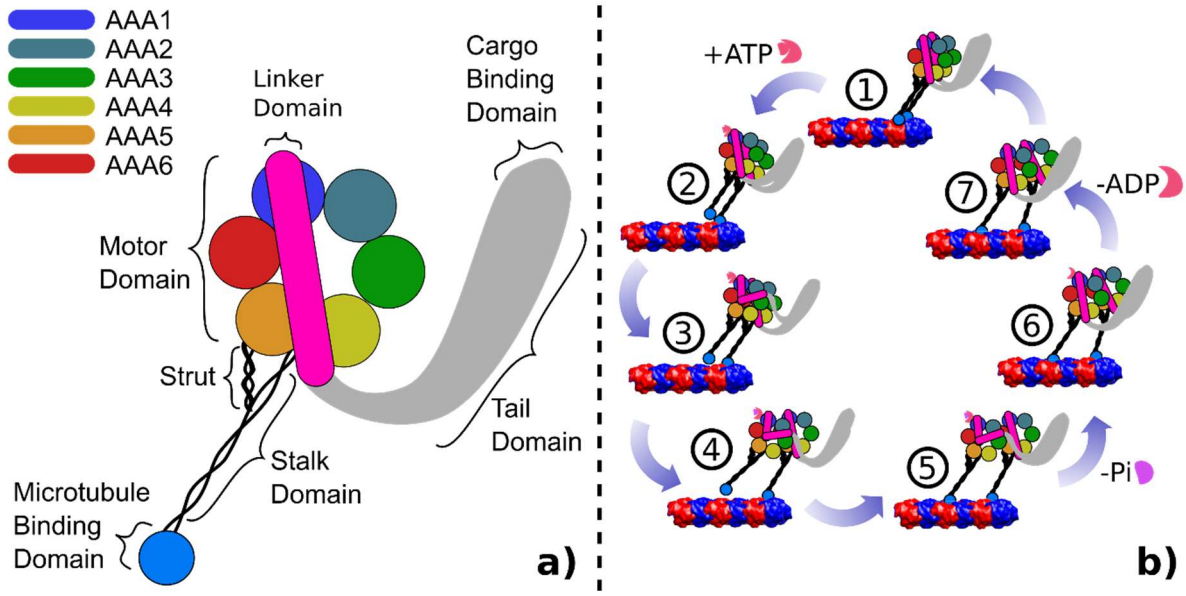

Figure 1. A schematic representation of a cytoplasmic dynein monomer and its associated kinetic cycle. **a)** A simplified representation of the monomer, showing the key domains known to affect the function of the motor. **b)** The kinetic cycle of the monomer and the relationship to the associated dimer.

With reference to a detailed analysis by Schmidt[5], simplified in Figure 1b, we briefly summarise the kinetic cycle of cytoplasmic dynein. Whilst in the 'post-powerstroke' state (1), the motor detaches from the MT track upon ATP binding. During this process, the linker domain is approximately straight, extending across to the AAA4 domain (2). Following detachment, the motor adopts the 'pre-powerstroke' conformation with the linker bending to a position between the AAA2/AAA3 domains (3) [6]. This conformation is retained as ATP hydrolysis occurs (4). When dynein rebinds to the MT track (5), a mechanical signal is transmitted along the stalk to the motor domain, which causes a subsequent rearrangement of the AAA+ ring. This triggers the release of the phosphate formed via ATP hydrolysis, and subsequently, the powerstroke occurs (6) [5]. ADP is then released from the hydrolysis site (7), leaving it available for another ATP molecule to bind, enabling the kinetic cycle to begin again in either the same monomer or the partner monomer.

To access the millisecond timescales intrinsic to motors such as dynein requires multiscale modelling to capture both local dynamics from fluctuations at the atomistic level and global the conformational changes of the entire motor complex. While atomistic MD simulations are well established, coarse-grained methods for capturing global dynamics of large complexes are less well developed. Fluctuating Finite Element Analysis (FFEA) is a mesoscopic model which represents biomolecules as viscoelastic continuum bodies that change shape due to thermal fluctuations [7], and which is capable of exploring micro/millisecond timescales for a motor such as dynein. FFEA uses the volumetric structure of the molecules together with continuum material parameters, such as elastic moduli and viscosities, to calculate the time evolution of the system subject to thermal fluctuations. FFEA calculations require these intrinsic material properties of the biomolecules to be explicitly specified to determine the magnitude and rate of thermally driven deformation occurring throughout a simulation. For the dynein conformations which are not bound to the MT track (which have atomistic co-ordinates available), we have developed a "bottom up" parameterisation based on more detailed atomistic MD simulations[2]. Here we show how our continuum mechanical models of cytoplasmic dynein monomers capture the conformational dynamics at the coarse-grained level. While our study

focuses on dynein as a model system, this methodology for obtaining mesoscale material parameters from atomistic simulation is potentially applicable to other systems, and offers a route to multi-scale modelling of biomolecular processes such as the stepping of molecular motors and the assembly of large protein complexes.

2. Material and Methods

2.1 Coarse-graining of atomistic MD simulations of dynein monomers

Kamiya *et al*, performed 200ns explicitly solvated atomistic MD simulations of two separate dynein conformations, providing 20,000 representative conformers for each state [2]. The two dynein models represented chimeric proteins structures, built using the linker and motor domains of a 2.8Å dynein structure combined with the MTBD from a 3.8Å structure, both solved by Kon *et al.*[3]. In the ADP model, an ADP molecule is present in each of the four available binding pockets (AAA1-AAA4). In the ATP model, however, a PO_3 group was added to the ADP molecule in AAA1 to form ATP, and the chloride ion and the closest water molecules were removed. The presence of either ADP or ATP in AAA1 can be thought of as representing a different phase of the dynein conformational cycle as shown in Figure 1b. The ATP model best represents the molecule immediately prior to the priming of the linker (Figure 1b:(2)), and the ADP model best represents the post-powerstroke state, although in the absence of the microtubule (Figure 1b:(1))[5,8].

To determine appropriate material parameters for FFEA simulations from the MD, it is necessary to identify the key degrees of freedom that must be captured to reproduce the dynamics of dynein at the mesoscale. Principal component analysis (PCA) can be used to decompose the two atomistic MD trajectories into a set of quasi-harmonic orthogonal motions, represented by eigenvectors, in order of their relative contribution to the overall conformational exploration, represented by the associated eigenvalues which have units of spatial variance[9]. This was performed using the pyPcazip toolkit [10], and indicated that the dominant contribution towards dynamical variance in the motor are fluctuations in the stalk and linker domains.

We therefore extracted the length and angular fluctuations of the stalk and linker domains from the atomistic trajectories as the basis for coarse-grained modelling, as shown in Figure 2. Time averaged structures were calculated from the set of 20,000 MD simulation frames using the MDAnalysis python package[11]. To calculate a distribution of angular fluctuations, we defined a single 'end-to-end' vector along the stalk structure, $\vec{v}_s$, and defined another vector, $\vec{v}_l$, along the linker domain. At each simulation frame we calculated the angular deviation from the average structures, θ_s and θ_l for the stalk and linker domains respectively, as shown in Figure 2. To calculate the fluctuations of the stalk contour length, Δl_s, and linker contour length, Δl_l, we decomposed $\vec{v}_s$ and $\vec{v}_l$ into vectors using further sets of intermediate residues, forming a piecewise representation of both the stalk and the linker domains. In the stalk, the residues defining the vectors were chosen via a simple linear interpolation along the stalk sequence, whereas in the linker (a more complex structure) the vectors were chosen by eye. The contour length fluctuations were then calculated as the sum of the lengths of each of these vectors minus the contour length from the average structure. Details of the residues used for the definition of each vector can be found in the Supplementary Information S2.

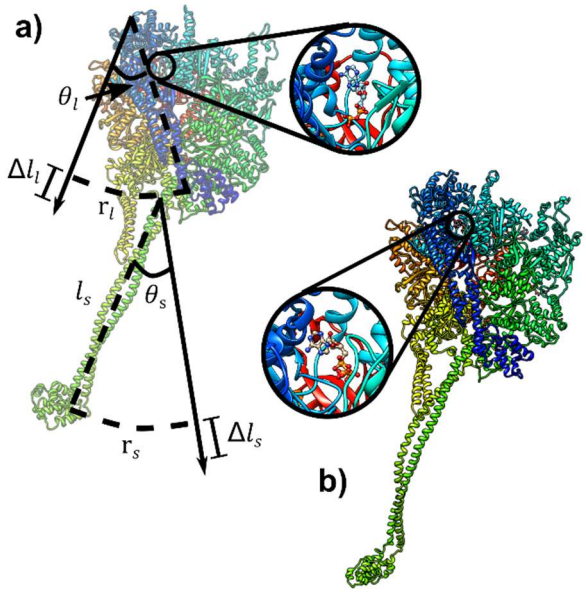

Figure 2. Atomistic models of the dynein monomers studied via MD simulation. **a)** The 'ADP' model, and **b)** The 'ATP' model, each with their respective ligand bound to the AAA1 hydrolysis site. Structural vector definitions are shown in **a)**.

2.2 Building a continuum finite element mesh of a dynein monomer

The FFEA simulation protocol represents biomolecules using a volumetric finite element mesh. We constructed a separate mesh from the time averaged structures of both the ADP and ATP models calculated from the MD trajectories. For each structure, we calculated an effective molecular surface using the 'Quick Surf' algorithm within VMD [12][13]. This resulted in a triangulated surface profile of 340,550 and 327,876 triangles for the ADP and ATP models respectively, both with minimum edge lengths significantly less than an angstrom. These surfaces were passed through an edge-collapse algorithm [14], which coarsens the surface by reducing the total number of triangles whilst at the same time keeping the local volume enclosed by the surface constant. In the resultant mesh, the minimum edge length was greater than 5Å for both the ADP and ATP models. Our finite element meshes are required to be mathematically closed surfaces, with a well-defined 'inside' and 'outside', so that a continuous, bounded volumetric profile can be defined for the molecule. However, the two-dimensional edge-collapse algorithm can lead to physically unrealistic local structures, such as interpenetrating faces. Additional manual processing of the triangulated surface was performed using the Blender modelling software package [15], enabling us to isolate these 'non-manifold' sections, delete them, and replace them with a consistent surface profile.

Within the atomistic structure the linker domain was so close to the motor domain that the surface profiling algorithm was unable to resolve the two sub-structures. To allow the linker to move relative to the motor domain, we again used Blender to manually disconnect the linker from the motor domain so that it is only attached to the motor domain at the base. The TETGEN software package [16] was then used to populate the enclosed volumes with the tetrahedra that constitute the 'elements' used in the finite element method. The progression of each model through these algorithms is shown in Figure 3.

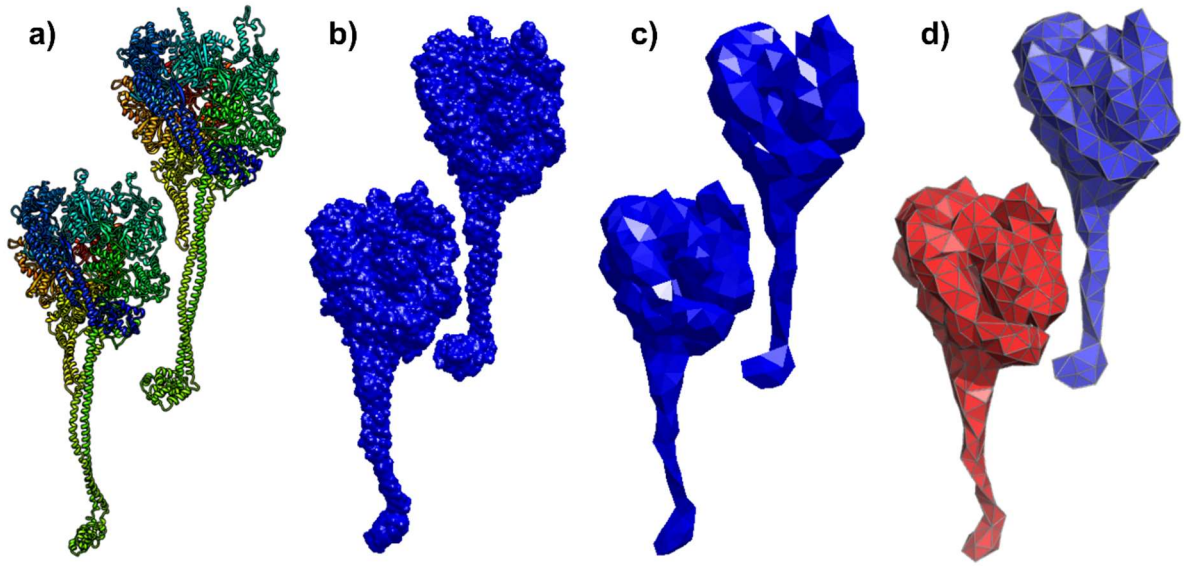

Figure 3. The FFEA meshing procedure performed for both the ADP model (top row) and ATP model (bottom row). **a)** The initial atomistic structures obtained via averaging the frames of the MD simulations. **b)** The initial surface profile of each model following 'Quick Surf' processing in VMD. **c)** The surface profile of each model following the application of the edge-collapse algorithm and corrections within Blender. **d)** The final, meshed FFEA models, each with a well-defined, closed volume filled with tessellating tetrahedra.

2.3 Fluctuating Finite Element Analysis of the dynein monomer

FFEA is a viscoelastic continuum simulation technique, which uses finite element analysis to solve the Cauchy momentum equation:

$$\rho \frac{D\vec{u}}{Dt} = \nabla \cdot \boldsymbol{\sigma}, \qquad (1)$$

where $\vec{u}$ is the continuous velocity profile over the object, $\frac{D}{Dt}$ is the material derivative, and the total stress $\boldsymbol{\sigma} = \boldsymbol{\sigma^e} + \boldsymbol{\sigma^v} + \boldsymbol{\sigma^t}$ is the three-dimensional stress tensor containing contributions from an elastic stress, a viscous stress and uniquely, a thermal stress. The elastic stress requires two elastic parameters: the Young's modulus (Y), and the Poisson ratio (ν). FFEA implements a linear viscous stress, such that the resulting viscous damping within the system is linearly proportional to the strain rate at any point. Finally, the combination of elastic and viscous stress components in series implies a Kelvin-Voigt constitutive model within FFEA, where the biomolecules fluctuate about a defined equilibrium structure without any permanent deformation.

To perform dynamic simulations using Eq. (1), FFEA includes an additional stochastic thermal noise in the form of a thermal stress, which is calculated to satisfy the fluctuation-dissipation theorem [7]. At the lengthscales we are simulating at and for the systems we are working with, it can be shown that the biomolecules are heavily overdamped in the degrees of freedom we

are interested in, and so we are able to neglect the inertial term on the LHS of Eq. (1). The application of finite element analysis to Eq. (1) in the absence of inertia yields:

$$\Lambda_{ij}\dot{x}_j + K_i(\vec{x}) = N_i \qquad (2)$$

where the summation convention is implied. Eq. (2) is a matrix equation defined for all the vertices of the volumetric mesh, where Λ_{ij} is the global viscosity matrix, $K_i(\vec{x})$ is the non-linear elasticity vector, and N_i is the coupled thermal noise vector. The indices i, j extend over all nodes and all directional components. As we have neglected the inertial terms, Eq. (2) represents a Brownian equation of motion for FFEA. Eq. (2) is a complete system of ODEs which can be solved numerically to obtain a trajectory for the nodes of the finite element mesh, corresponding to the motion of the biomolecule as represented in a continuum mechanical framework.

All FFEA simulations within this study were performed using shared-memory parallelisation on 4 AMD Opteron Model 6376 processors. Each simulation was performed with a different set of elastic material parameters, which gave us the additional capability to slightly optimise our integration timestep for each simulation, with a maximum timestep $dt = 10fs$ used for the most flexible system, and a minimum timestep $dt = 1fs$ used for the most rigid system. To maximise the speed of dynamical convergence for our simulations without affecting the motor conformations sampled, we uniformly reduced the effective background viscosity of our simulations to $\mu_{ADP} = 53.0$kPa.ns for the ADP model, and $\mu_{ATP} = 55.6$kPa.ns for the ATP model. With these resources and parameters, each simulation required approximately 1 day to produce a 1μs FFEA trajectory containing 10,000 simulation frames.

2.4 Analysis of FFEA Simulations

To analyse the trajectories of our FFEA simulations, and compare them with the atomistic simulations from which they were parameterised, we generated an interpolative coordinate mapping from the nodes of the FFEA structure to the atoms of the corresponding MD models. This mapping takes the form of a matrix transformation of the form:

$$\vec{x}_A = \boldsymbol{M}\vec{x}_N \qquad (3)$$

where $\vec{x}_N$ is the vector of all FFEA node coordinates and $\vec{x}_A$ is the vector of all associated atomic coordinates. As there are potentially different numbers of atoms and nodes, $\boldsymbol{M}$ is non-square and thus does not have a unique form**.** However**,** due to the topological structure of FFEA meshes remaining constant over the course of a simulation, we can use the initial states of the FFEA and atomistic structures to algorithmically calculate a unique interpolation for each atom, using the edge vectors of the single FFEA element which contains the atom[7,17]. Hence, $\boldsymbol{M}$ is a highly sparse mapping matrix from the FFEA structure to the atomistic equivalent, and forms a largely interpolative (and hence, stable) mapping for any FFEA mesh configuration.
Using this mapping, we were then able to calculate the 'equivalent' MD structure for any given FFEA trajectory frame. Applying the map to each frame of an FFEA trajectory therefore produces a pseudo-atomistic trajectory which retains the mesoscopic dynamics of the FFEA simulation by interpolating the effective atomic motions. This procedure enabled us to perform the same analysis to the FFEA trajectories as to the MD trajectories for consistent comparison.

2.5 Assessment of time-scales relevant to dynein dynamics from Euler-Beam theory

To obtain an order of magnitude estimate for the timescales associated with thermal fluctuations of the dynein stalk, we can approximate this object as an ideal linear beam and estimate the associated timescales analytically with Euler-Bernoulli beam theory [18]. For both an unrestrained beam, and for a beam rigidly restrained at one end, the motion associated with the longest timescale will be a first-order bend, which is consistent with our initial principal component analysis (see Sections 2.1 and 3.3).

A linear elastic constant k_e associated with this degree of freedom can be found by associating this motion with the bending modulus, E_b:

$$E_b = \frac{l^3}{4w^4} k_e \tag{4}$$

where w is the width and l the beam length and E_b is the bending modulus (equivalent to the Young's modulus in an ideal case). Within the MD simulations the dynein stalk is immersed in explicit water, which exerts a viscous drag given by [19]:

$$\lambda \approx \pi \mu l \tag{5}$$

where this approximation can be made due to the long and thin dimensions of the dynein system (specifically $l = 12$nm and $w = 1.5$nm). For an idealised beam with equivalent dimensions to the dynein stalk and assuming $E_b \approx 1$GPa to be representative of globular proteins [20] and setting the dynamic viscosity $\mu = 1$ MPa.ns [21], the relaxation timescale of the highest amplitude global mode (stalk bending):

$$\tau = \frac{\lambda}{k_e} = \frac{\pi}{4}\left(\frac{l}{w}\right)^4 \frac{\mu}{E_b} = 3.22ns \tag{6}$$

Consequently, we would expect a 200ns simulation to contain approximately 60 independent observations of the slowest motion in the system. Robust statistical analysis requires ~1000 observations, and so although our fluctuation distributions may have converged to relatively constant values, the effective elasticities we extract from these data should be considered as a lower bound.

We used the FFEA timescale calculator to determine the required simulation times required for statistical convergence of averages over conformational space[7]. With reference to Eq. (2), this sub-routine of the FFEA algorithm performs an eigen-decomposition of the matrix Λ_{ij} together with the matrix resulting from the linearization of the elasticity vector K_i, which results in a spectrum of timescales corresponding to the dynamical normal modes of the system. Using the representative values $Y = 1$ GPa and $\mu = 1$ MPa.ns, we found that the longest timescales in the system were $\tau_{ADP} = 3.08$ ns and $\tau_{ATP} = 4.52$ ns, which supports our theoretical result in Eq. (6). For the lowest value of Young's modulus used in our simulation series, $Y = 0.40$GPa, which corresponds to the slowest exploration of conformational space of all our simulations, we found that the longest timescales in the system (with modified external

viscosity) were $\tau_{ADP} = 0.17\,\text{ns}$ and $\tau_{ATP} = 0.26\,\text{ns}$. Within a $1\,\mu\text{s}$ simulations, then, we therefore expected to obtain ~6000 independent observations of the slowest mode for the ADP model and ~4000 for the ATP model, which is sufficient for statistical convergence of averages over conformational space.

2.6 Error propagation from MD into FFEA

The coarse-grained nature of FFEA simulations means that we can comfortably run simulations long enough to achieve statistical convergence. We therefore estimate the largest error in our parameterisation procedure by considering the number of independent conformers (from Eq. (6)) observed in the short (200ns) timescales of the original MD simulations. We propagate these errors forward into errors in subsequent FFEA parameterisation values using the measured linear correspondence between the appropriate parameters, which is visualised in Figure 5.

2.7 Principal Component Analysis of FFEA and MD Simulations

To compare the parameterised FFEA trajectories to the original MD trajectories, we performed PCA on both datasets individually and compared their resulting sets of eigenvectors. pyPcazip [10] was used to determine the eigenvectors corresponding to both the original MD trajectories, and those corresponding to the FFEA trajectories represented as psuedo-MD trajectories via our interpolative mapping procedure. The atomic coordinates act as a mutual coordinate system, allowing us to directly calculate the inner products between each pair of eigenvectors, telling us how well the two simulations correspond to one another in terms of dynamical variance. For computational efficiency, all PCA was performed using the backbone Cα atoms only in both the original MD trajectories and the FFEA pseudo-MD trajectories.
Following this direct comparison, we combined the FFEA and MD trajectories of each model (ADP and ATP) into a single combined set of frames and performed PCA on this dataset. This combined trajectory yields a mutual eigenspace with which both the FFEA and MD eigenspaces can be independently compared. This was used to determine the respective magnitudes of the dominant modes obtained from FFEA and MD simulations, and compare the dynamic range of motion available in each technique following parameterisation.

3. Results

3.1 Linear elastic constants for the longitudinal and angular fluctuations of the dynein stalk and linker domains extracted from MD simulations

Figure 4 shows the probability distributions of the contour length and angular fluctuations for the linker and stalk domains for both the ADP and ATP models. For the ADP model contour length fluctuations, the distributions exhibit the expected distributions for linear elastic behaviour; a Gaussian distribution for the length fluctuations with associated linear stiffnesses k_x. For the linker angular fluctuations in both the ADP and ATP models, we observe behaviour of the form:

$$p(\theta) \approx \frac{K_\theta}{k_B T}\theta \exp\left(-\frac{K_\theta \theta^2}{2k_B T}\right) \tag{7}$$

which is a Rayleigh distribution with associated angular stiffness K_θ. As each of our angles θ_s and θ_l are reduced from two spatial degrees of freedom around the equilibrium structures into a single angular variable, Eq.(7) is the equivalent distribution for the purely positive coordinate. While both states exhibit simple elastic behaviour for the angular fluctuations, the contour fluctuations in the ATP model exhibit a bimodal Gaussian distribution, indicating the presence of two equilibrium states within the molecule. Nevertheless, for these dynein monomers, the conformational variation is dominated by angular motion (see Table 1), and we are therefore justified in approximating this more complex behaviour using a linear model with a single variable. However, it is important to carefully assess the validity of the elastic approximation when parameterising FFEA models from atomistic simulations by plotting the relevant probability distributions. PCA based statistics can also reveal other useful characteristics from the MD, e.g. plotting the amplitude of a mode as a function of simulation time can reveal whether a particular bimodal distribution arises from rapid fluctuations between two states, or whether it results from slow conformational rearrangements over the timescale of the MD simulation[9].

To extract linear elastic constants for each fluctuation parameter, we relate the length and angular fluctuations to the expected thermal energy using the equipartition theorem. For the contour length fluctuations:

$$k_l = \frac{k_B T}{\langle \left(l - \bar{l}\right)^2 \rangle} \tag{8}$$

where $\bar{l}$ represents the total mean of the distributions shown in Figures 5a and 5b, and $k_B T$ is the Boltzmann energy factor. For the angular fluctuations, which correspond to two degrees of freedom, we can define an elastic constant k_r with the same units as k_θ by converting our angular fluctuations into fluctuations in the coordinate r (see Figure 2). With $r = \bar{l}\theta$, we obtain:

$$k_r = \frac{2k_B T}{\bar{l}^2 \langle \theta^2 \rangle} \tag{9}$$

$k_l$wand k_r now have the same units, which enables a direct comparison between the angular and contour length fluctuations. The linear elastic constants and corresponding fluctuation standard deviations extracted from the distributions are shown in Table 1.

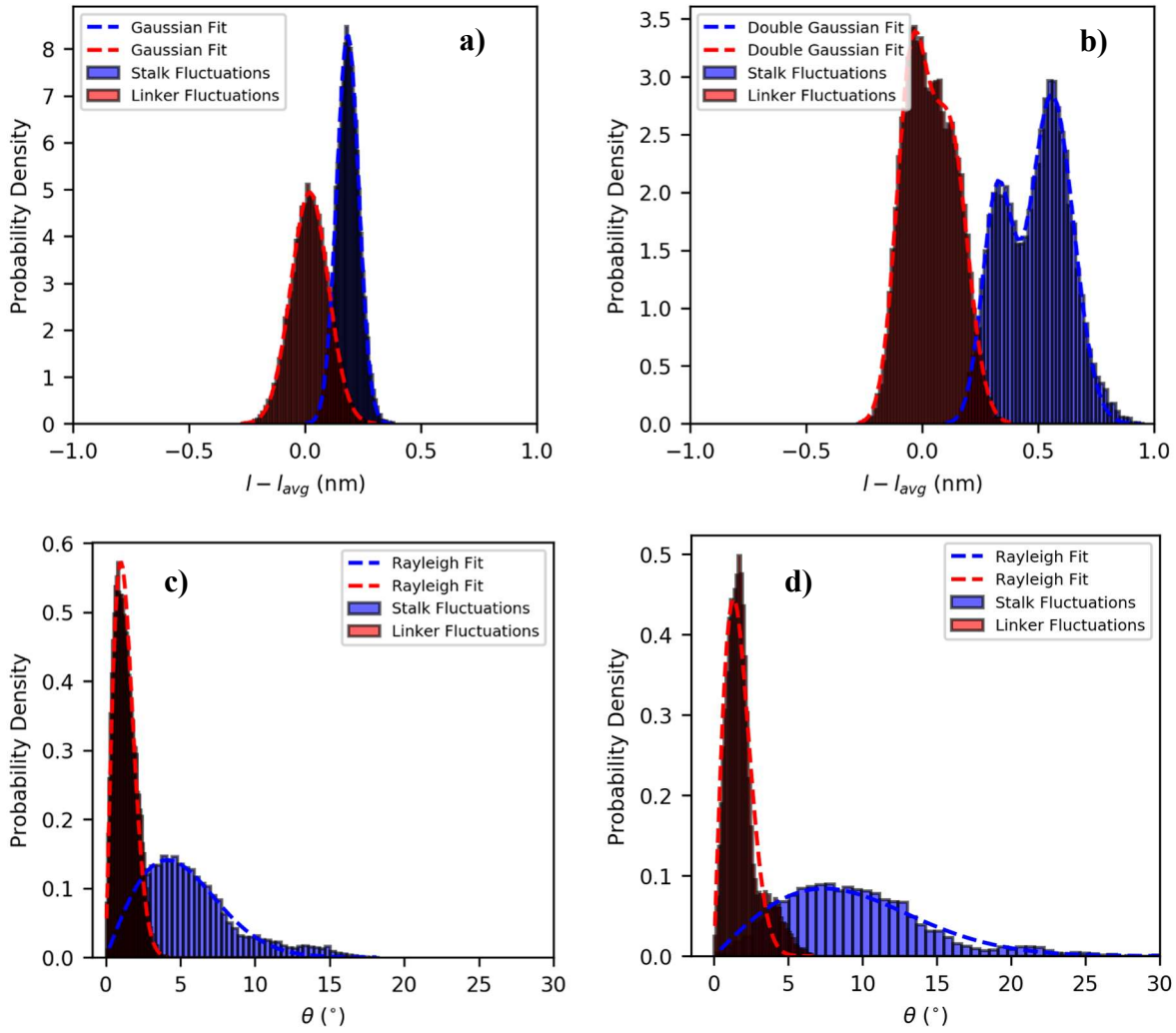

Figure 4. The probability distributions corresponding to the parameter fluctuations extracted from the MD simulations. **a)** ADP contour length fluctuations. **b)** ATP contour length fluctuations. **c)** ADP angular fluctuations. **d)** ATP angular fluctuations. l_{avg} corresponds to the contour lengths in the average structure, not the average contour length, which is why the contour length distributions are not centred on zero.

Table 1 shows that the motion associated with angular fluctuations is responsible for a greater amount of spatial exploration than the contour length fluctuations, as expected for long, thin objects such as the stalk and linker domains. Moreover, the effective angular stiffness of the linker domain is approximately 23 times greater than the linker in the ADP model, and 26 times greater in the ATP model, indicating that the stalk is a much more geometrically flexible object. Finally, we note that the ADP model stalk angular stiffness is approximately 2.6 times greater than that of the ATP model, and the ADP model linker angular stiffness is 2.2 times greater than the ATP model, which may indicate that the presence of ATP in the AAA1+ domain in dynein may lead to an increase in flexibility delocalised over the entire molecule. Further details regarding the statistical convergence of these distributions is provided in Supplementary Information S3.

Model	ADP		ATP	
	Stalk	Linker	Stalk	Linker
Linear Elastic Constant				
Contour Length (pN/nm)	1700 ± 317	627 ± 114	199 ± 36	354 ± 64
Angular (pN/nm)	4.1 ± 0.7	93 ± 17	1.6 ± 0.3	42 ± 8
Standard Deviation				
Contour Length (nm)	0.048 ± 0.004	0.081 ± 0.007	0.14 ± 0.01	0.11 ± 0.01
Angular (nm)	1.4 ± 0.1	0.30 ± 0.03	2.3 ± 0.2	0.44 ± 0.04

Table 1. Linear elastic constants and the associated fluctuation standard deviations extracted from the dynamical variable fluctuation distributions calculated from atomistic MD. The two representations are equivalent and can be interchanged using Eq. (8) and Eq. (9).

3.2 Angular fluctuations of the dynein stalk and linker domains in FFEA

To systematically parameterise our FFEA models, we first performed seven $1\,\mu$s FFEA simulations of both the ADP and ATP models for different values of the Young's modulus, Y, ranging from 0.1MPa and 1GPa and set homogeneously throughout the mesh. To account for the second required elastic parameter, a Poisson ratio, ν, of 0.35 was used throughout in accordance with the preliminary findings of Oliver[14]. To compare these coarse-grained simulations directly with the MD data, we applied the coordinate mappings described in see Section 2.4 to the FFEA trajectories in order to generate the equivalent, interpolated MD trajectories. We thereby obtained angular fluctuation distributions for the stalk and linker domains for direct comparison with the original atomistic models.

From linear elastic theory, we would expect the stiffness to be proportional to the Young's modulus. Assuming equipartition, we therefore expect:

$$\langle \theta^2 \rangle \propto \frac{k_B T}{Y} \tag{10}$$

Taking logarithms of both sides then gives:

$$ln\left(\langle \theta^2 \rangle\right) = -ln\,(Y) \; + \; c \tag{11}$$

where we have absorbed $k_B T$ into c, a general constant. Plotting the logarithms of the Young's moduli against the logarithm of the measured angular variances from our FFEA simulations gives the expected linear dependence, as shown in Figure 5. This implies that our simulations have indeed converged to statistical ergodicity. Linear regression using Eq. (11) enables us to

extract the Young's moduli which would correspond to the various fluctuation magnitudes calculated from the original MD simulations.

The theoretical Young's modulus is an intrinsic property of an elastic object and thus independent of its geometry. That our moduli values are different for both length and angular fluctuations in the same sub-structure immediately indicates that a more complex system of internal interactions exists within the dynein stalk and linker domains that is difficult to account for with an isotropic continuum model. Given that our FFEA structures were calculated explicitly from the surface profile of the average MD structure, indicating that we have the correct representative geometry, it is likely that the difference between contour length and angular moduli emerges from anisotropic elasticity existing at the atomic level. While in principle it is possible to include this by defining an appropriate anisotropic constitutive model of elasticity within the FFEA continuum model, we can neglect this effect here because, as previously noted, angular fluctuations dominate the motion.

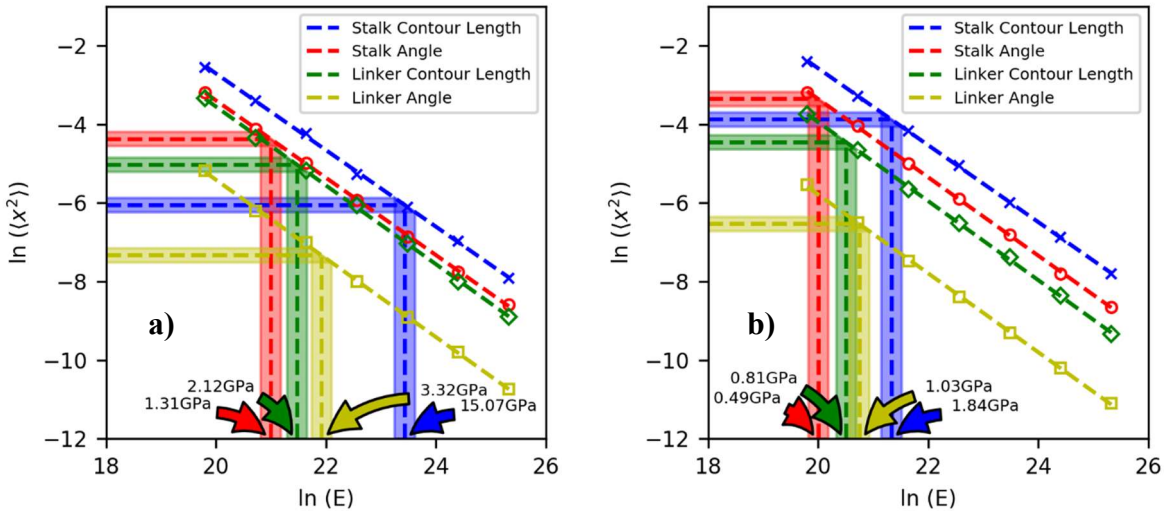

Figure 5. The relationship between the homogeneous Young's moduli and measured fluctuation variances (in both length and angular coordinates) following a suitably converged FFEA simulation of the dynein monomers for **a)** the ADP model and **b)** the ATP model. Using the fluctuation variances calculated from the MD simulation, we can determine the effective Young's moduli required to reproduce the relevant atomistic dynamics within the coarsened FFEA framework.

For the angular fluctuations, the Young's modulus of the linker domain is greater than that of the stalk in both the ADP and ATP models. This indicates a stiffer internal structure of the linker relative to the stalk. The Young's modulus of the ATP model is reduced by a factor of approximately 2.7 for the stalk domain, and 3.2 for the linker domain compared to the ADP model, indicating that our parameter extraction for FFEA can indeed capture the dynamic differences between the ADP and ATP states observed in the atomistic MD.

3.3 Dynamical modes of inhomogeneously parameterised FFEA simulations compared to MD simulations

PCA performed on the atomistic MD simulations indicates that the main contribution to the dynamics of ADP and ATP models of dynein comes from angular fluctuations of the stalk and linker domains, and our analysis of the fluctuations has provided quantitative values for the appropriate structural components (see Table 1). Figure 6 shows the distribution of Young's moduli across the dynein molecule in both the ADP and ATP models when parameterised using these optimised values in each structural subunit. The motor domains of each model are parameterised with the mean of the linker and stalk domain moduli.

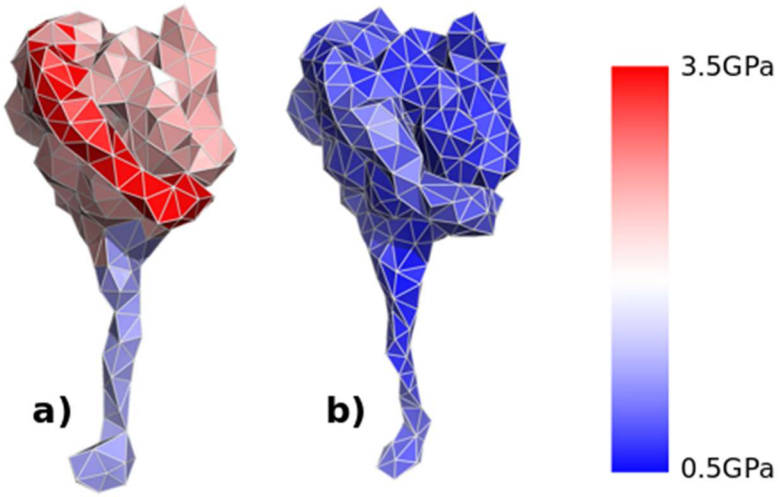

Figure 6. A visualisation of the mechanical parameterisation of **a) t**he ADP model and **b) t**he ATP model. The motor domain of each model is homogeneously parameterised as the mean value between the stalk and linker domains.

We performed $1\mu s$ FFEA simulations of these inhomogeneously parameterised models and used our interpolative mapping algorithm to again generate pseudo-atomistic trajectories for direct comparison with the original MD simulations. To assess the ability of this FFEA model to capture the dynamics of the dynein monomer at the mesoscale, given our parameterisation, we performed various forms of PCA on both of these FFEA trajectories and compared the eigensystems obtained with those calculated from the atomistic MD to determine whether the dynamical motions represented by the eigensystems are equivalent.

Table 2 shows the inner products between the eigenvectors of three most significant modes resulting from both the ADP and ATP model trajectories simulated with MD and FFEA. These correlations show the mathematical overlap between the 'shapes' of the modes. The clustering of high correlations close to the diagonal indicates a good agreement between the two different modelling methods, particularly for the two most significant modes, which represent stalk bending motions. The respective eigenvalues for each of the modes and animations of their dynamic representation are provided as Supplementary Information.

Model		ADP			ATP		
Domain		Stalk + MTBD			Stalk		
Simulation		FFEA			FFEA		
	Mode	1	2	3	1	2	3
MD	1	**0.82**	0.33	0.25	**0.82**	0	**0.39**
	2	0.34	**0.92**	0.08	0.1	**0.95**	0.14
	3	0.33	0.07	**0.77**	0.29	0	0.19

Table 2. Inner product matrices calculated from PCA of the entire dynein monomer of both the ADP and ATP models. FFEA simulations are converted to pseudo-atomistic trajectories for comparison with MD simulations. The most significant 3 mode overlaps of each matrix are highlighted in white-bold text.

To assess the ability of the FFEA to reproduce the atomistic trajectories for each sub-structure, we separated the stalk and linker domains into separate trajectories and performed PCA on each of the domains individually. The inner product matrices comparing FFEA and MD are shown in Tables 3 and 4.

Model		ADP								
Domain		Stalk + MTBD			Stalk			Linker		
Simulation		FFEA			FFEA			FFEA		
	Mode	1	2	3	1	2	3	1	2	3
MD	1	**0.64**	0.34	0.5	**0.95**	0.13	0.04	0.37	0.27	**0.5**
	2	0.51	0.27	**0.7**	0.12	**0.96**	0.13	0.11	0.44	0.2
	3	0.46	**0.83**	0.02	0.09	0.11	**0.88**	0.05	**0.64**	**0.55**

Table 3. Inner product matrices calculated from PCA of both the stalk and linker domains of the ADP model. FFEA simulations are converted to pseudo-atomistic trajectories for comparison with MD simulations. The most significant 3 mode overlaps of each matrix are highlighted in white-bold text.

Model		ATP								
Domain		Stalk + MTBD			Stalk			Linker		
Simulation		FFEA			FFEA			FFEA		
	Mode	1	2	3	1	2	3	1	2	3
MD	1	**0.47**	0.02	**0.33**	**0.64**	0.2	**0.39**	0.44	0.25	**0.71**
	2	0.18	**0.85**	0.07	0.18	0.07	0.01	**0.59**	**0.58**	0.18
	3	0.29	0.18	0.14	0.24	**0.79**	0.07	0.05	0.34	0.14

Table 4. Inner product matrices calculated from PCA of both the stalk and linker domains of the ATP model. FFEA simulations are converted to pseudo-atomistic trajectories for comparison with MD simulations. The most significant 3 mode overlaps of each matrix are highlighted in white-bold text.

We can see from Tables 3 & 4 that the spectrum of dynamical behaviour of the stalk domain appears to be well captured by the mesoscale models. The linker exhibits more complex dynamic behaviour, however, there is still significant overlap between the top modes. Inclusion of the MTBD as part of the stalk reduces the overall overlap between modes from the two simulation techniques, because the hinge formed by the junction between the stalk and the MTBD[22] decouples their relative motion. The strong correlations we obtain between the eigenvectors for the global dynamics of dynein at the atomistic and coarse-grained levels is most likely due to the stalk dynamics being the dominating source of flexibility in the molecule.

3.4 Dynamical range of inhomogeneously parameterised FFEA simulations compared to MD simulations

To validate not only the shape of the modes, but their relative magnitude, we cannot directly compare the eigenvalues of each simulation as this comparison itself depends on how similar the shapes of modes are. To compensate for this, we combined the FFEA and MD trajectory frames into a single dataset for both the ADP and ATP models, and performed further PCA on these. This PCA decomposition provides not only a mutual coordinate system, but a mutuak eigenspace with which both the FFEA and MD simulations can be independently compared.

We used pyPcazip to calculate the eigenspace overlap between both the FFEA and MD eigensystems and the combined eigensystem for both the ADP and ATP models. This overlap is the normalised sum of inner products between each of the pairs of eigenvectors, the results of which are shown in Table 5. Similar to the results shown in Table 2, we observe a high level of overlap for both simulation methods, but particularly for the ADP model, which is less flexible.

Model	ADP		ATP	
Domain	Whole		Whole	
Simulation	MD	FFEA	MD	FFEA
Combined	0.999	0.923	0.969	0.854

Table 5. The subspace overlap for each model (ADP/ATP) between the individual PCA eigensystems for each simulation trajectory (MD/FFEA), and the combined PCA eigensystem for both simulation trajectories. Overlaps were calculated using the three most significant modes from each eigensystem.

We then compared the range of conformational space explored by each simulation technique by projecting the first two eigenvectors of each independent simulation into the combined eigenspace for each model. Figure 7 visualises the distribution of these projections as normalised two-dimensional heatmaps.

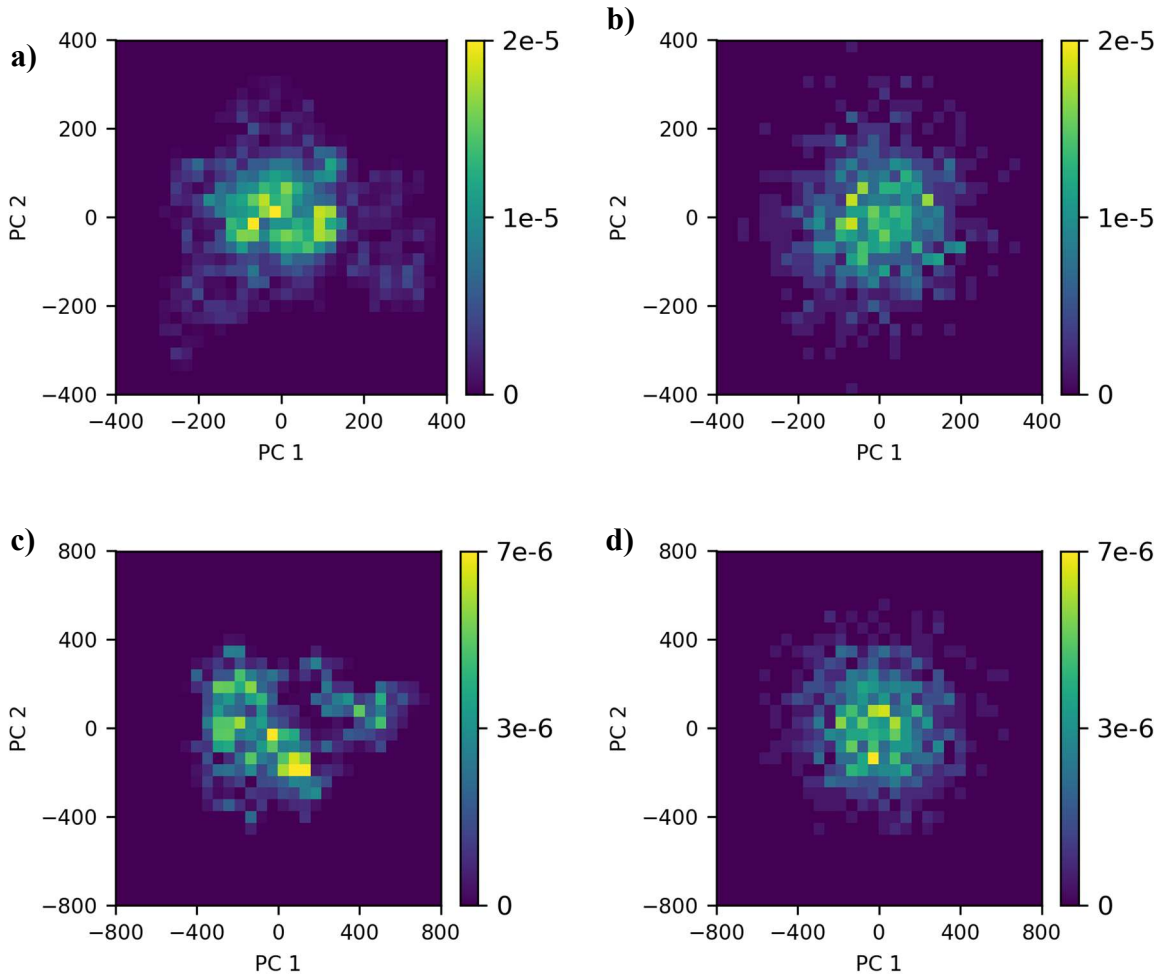

Figure 7. Normalised histograms of the frequency distribution of projections between the individual simulation eigenspaces and the combined trajectory eigenspaces. **a)** The MD simulation of the ADP model. **b)** The FFEA simulation of the ADP model. The FFEA simulation of the ADP model. **c)** The MD simulation of the ATP model. **d)** he FFEA simulation of the ATP model.

While the 2D distributions for the ADP model in MD (Fig 7a) and FFEA (Fig 7b) are very similar, there are differences for the ATP models, due to bimodality in the MD simulations (Fig 7c) that are not captured by the FFEA model (which will always show Gaussian fluctuations around the average structure). However, the ATP model does show a distribution with wider dynamic range than the ADP using both MD and FFEA, indicating that it is significantly more flexible when ATP is bound. This indicates that our FFEA parameterisation has successfully reproduced not only the principle shapes of the modes from the original MD, but also the relative magnitudes of flexibility in those modes.

4. Discussion

Using the parameterisation methodology presented here, our multi-scale approach to the simulation of dynein enables us to explore far longer timescales than would be possible with a single scale, atomistic simulation. Previous experimental work has shown how the motor is able to walk along the track, and these images will be used to validate subsequent calculations

of the walking mechanism for dimeric dynein [22] [23]. Further calculations in the presence of cargoes and accessory binding partners [24] can now also be considered as computationally feasible. For example, dynactin was recently observed to recruit as many as four dynein monomers in the form of two dimers[25][26], but the importance of these additional dyneins to the performance of the motor complex remains poorly understood.

However, as we learn more about the mechanics and regulation of dynein, additional parameterisation using atomistic models may be necessary. Recent work on cytoplasmic dynein tension sensing [4] has shown that the two α-helices which make up the stalk domain of the motor sense tension by sliding relative to one another. This sliding is also known to alter the molecular registration of the MTBD, and change its affinity to the MT track. For these effects to be captured, we will need atomistic simulations to determine how MT binding changes with tension, and to incorporate these effects implicitly in our coarse-grained models.

5. Conclusions

We have presented a parameterisation scheme that enables multi-scale simulations spanning the atomistic to continuum regimes. From an atomistic MD trajectory, we used PCA to isolate the major modes of flexibility, and used these as a basis for coarse-graining. We extract the relevant stiffnesses from atomistic simulations, and used them to benchmark a series of approximately equivalent mesoscale FFEA simulations. We subsequently found the appropriate FFEA material parameters for each degree of freedom considered, and ran further FFEA simulations for comparison with the original MD. We found that parameterisation based on these minimal degrees of freedom retains the dominant dynamical behaviour at the mesoscale.

Various approximations have been made as we moved from the atomistic to continuum regimes. Firstly, as this is a 'bottom-up' approach, we rely on high-resolution atomistic MD trajectories to capture the dynamics flexibility of the motor in each conformational state. Whilst we have been able to accurately parameterise the FFEA models based on the original MD simulations, atomistic simulations generally suffer from limited sampling due to the enormous computational expense of the calculations, thus under-estimating the biomolecular flexibility, and are also subject to caveats associated with empirical forcefields. However, through consideration of the geometry of the dynein monomers, we are confident that the atomistic MD does indeed reproduce the major modes of flexibility of the dynein motor. Moreover, the linear (harmonic) approximation will not always hold for biomacromolecules, as these are held together by a myriad of weak non-bonded interactions that are inherently anharmonic in character. The validity of this approximation can be assessed by inspection of the probability distributions associated with each mode (as in Figure 4). Here, we have presented a basic protocol for obtaining continuum parameters from atomistic models. However, more sophisticated treatments such as the representation of switching between different discrete protein conformational states, inclusion of constitutive models that allow for plastic deformation, and anisotropic material properties are all possible within the FFEA framework.

Funding

This work was supported by the BBSRC Japan Partnering Award to the Astbury Centre (University of Leeds, UK) and the Institute for Protein Research (Osaka University, Japan) [Grant: BB/M027953/1], with additional supplementation from participating institutions. Additional support was made by the EPSRC through a DTA to Ben Hanson.

Bibliography

[1] Y. Kinoshita, T. Kambara, K. Nishikawa, M. Kaya, H. Higuchi, Step Sizes and Rate Constants of Single-headed Cytoplasmic Dynein Measured with Optical Tweezers, Sci. Rep. 8 (2018) 1–14. doi:10.1038/s41598-018-34549-7.

[2] N. Kamiya, T. Mashimo, Y. Takano, T. Kon, G. Kurisu, H. Nakamura, Elastic properties of dynein motor domain obtained from all-atom molecular dynamics simulations, Protein Eng. Des. Sel. 29 (2016) 317–326. doi:10.1093/protein/gzw022.

[3] T. Kon, T. Oyama, R. Shimo-Kon, K. Imamula, T. Shima, K. Sutoh, G. Kurisu, The 2.8A crystal structure of the dynein motor domain, Nature. 484 (2012) 345–350. doi:10.1038/nature10955.

[4] L. Rao, F. Berger, M.P. Nicholas, A. Gennerich, Molecular mechanism of cytoplasmic dynein tension sensing, Nat. Commun. 10 (2019) 3332. doi:10.1038/s41467-019-11231-8.

[5] H. Schmidt, Dynein motors: How AAA+ ring opening and closing coordinates microtubule binding and linker movement, BioEssays. 37 (2015) 532–543. doi:10.1002/bies.201400215.

[6] H. Schmidt, R. Zalyte, L. Urnavicius, A.P. Carter, Structure of human cytoplasmic dynein-2 primed for its power stroke, Nature. 518 (2015) 435–438. doi:10.1038/nature14023.

[7] A. Solernou, B.S. Hanson, R.A. Richardson, R. Welch, D.J. Read, O.G. Harlen, S.A. Harris, Fluctuating Finite Element Analysis (FFEA): A continuum mechanics software tool for mesoscale simulation of biomolecules, PLOS Comput. Biol. 14 (2018) e1005897. doi:10.1371/journal.pcbi.1005897.

[8] A. Šarlah, A. Vilfan, The winch model can explain both coordinated and uncoordinated stepping of cytoplasmic dynein, Biophys. J. 107 (2014) 662–671. doi:10.1016/j.bpj.2014.06.022.

[9] S.A. Harris, C.A. Laughton, A simple physical description of DNA dynamics: Quasi-harmonic analysis as a route to the configurational entropy, J. Phys. Condens. Matter. 19 (2007). doi:10.1088/0953-8984/19/7/076103.

[10] A. Shkurti, R. Goni, P. Andrio, E. Breitmoser, I. Bethune, M. Orozco, C.A. Laughton, pyPcazip: A PCA-based toolkit for compression and analysis of molecular simulation data, SoftwareX. 5 (2015) 44–50. doi:10.1016/j.softx.2016.04.002.

[11] R.J. Gowers, M. Linke, J. Barnoud, T.J.E. Reddy, M.N. Melo, S.L. Seyler, J. Domański, D.L. Dotson, S. Buchoux, I.M. Kenney, O. Beckstein, MDAnalysis: A Python Package for the Rapid Analysis of Molecular Dynamics Simulations, (2016) 98–105. http://conference.scipy.org/proceedings/scipy2016/oliver_beckstein.html%5Cnhttp://conference.scipy.org/proceedings/scipy2016/pdfs/oliver_beckstein.pdf.

[12] M. Krone, J. Stone, T. Ertl, K. Schulten, Fast Visualization of Gaussian Density Surfaces for Molecular Dynamics and Particle System Trajectories, Eurographics Conf. Vis. 2012 (2012) 67–71. doi:10.2312/PE/EuroVisShort/EuroVisShort2012/067-071.

[13] W. Humphrey, A. Dalke, K. Schulten, VMD: Visual molecular dynamics, J. Mol. Graph. 14 (1996) 33–38. doi:10.1016/0263-7855(96)00018-5.

[14] R.C. Oliver, A stochastic finite element model for the dynamics of globular proteins, 2013. http://etheses.whiterose.ac.uk/5555/1/Oliver Robin - eThesis.pdf.

[15] Open-source, Blender, (2017). https://www.blender.org/.

[16] H. Si, Hang, TetGen, a Delaunay-Based Quality Tetrahedral Mesh Generator, ACM

Trans. Math. Softw. 41 (2015) 1–36. doi:10.1145/2629697.
[17] B.S. Hanson, Mesoscale Modelling of Cytoplasmic Dynein using Fluctuating Finite Element Analysis, University of Leeds, 2018. http://etheses.whiterose.ac.uk/id/eprint/19398.
[18] J.M. Gere, S.P. Timoshenko, Mechanics of materials, 6th ed., Brooks/Cole-Thomas Learning, 2004.
[19] R.G. Cox, The motion of long, slender bodies in a viscous fluid. Part 1: General Theory, J. Fluid Mech. 44 (1970) 791–810.
[20] J. Howard, Mechanics of Motor Proteins and the Cytoskeleton., Sinauer Associates, Sunderland (Massachusetts), 2001.
[21] J.R. Rumble, CRC handbook of chemistry and physics., 99th ed., CRC Press LLC, 2018. https://books.google.co.uk/books?id=qXG9tAEACAAJ&dq=isbn:9781138561632&hl=en&sa=X&ved=0ahUKEwjM9_jU4LThAhUytXEKHddVDyYQ6AEIKjAA (accessed June 7, 2019).
[22] H. Imai, T. Shima, K. Sutoh, M.L. Walker, P.J. Knight, T. Kon, S.A. Burgess, Direct observation shows superposition and large scale flexibility within cytoplasmic dynein motors moving along microtubules, Nat. Commun. 6 (2015) 1–11. doi:10.1038/ncomms9179.
[23] A.J. Roberts, T. Kon, P.J. Knight, K. Sutoh, S.A. Burgess, Functions and mechanics of dynein motor proteins, Nat. Rev. Mol. Cell Biol. 14 (2013) 713–726. doi:10.1038/nrm3667.
[24] S.L. Reck-Peterson, W.B. Redwine, R.D. Vale, A.P. Carter, The cytoplasmic dynein transport machinery and its many cargoes, Nat. Rev. Mol. Cell Biol. 19 (2018) 382–398. doi:10.1038/s41580-018-0004-3.
[25] L. Urnavicious, C.K. Lau, M.M. Elshenawy, E. Morales-Rios, C. Motz, A. Yildiz, A.P. Carter, Cryo-EM shows how dynactin recruits two dyneins for faster movement, 554 (2018) 202–6. doi:10.1016/j.artmed.2015.09.007.Information.
[26] D.A. Grotjahn, S. Chowdhury, Y. Xu, R.J. McKenney, T.A. Schroer, G.C. Lander, Cryo-electron tomography reveals that dynactin recruits a team of dyneins for processive motility, Nat. Struct. Mol. Biol. 25 (2018) 203–207. doi:10.1038/s41594-018-0027-7.
[26] [Dataset] B.S. Hanson, S Iida, D.J. Read, O.G. Harlen, G. Kurisu, H. Nakamura, S.A. Harris, Data for: Continuum Mechanical Parameterisation of Cytoplasmic Dynein from Atomistic Simulation, Mendeley Data, 2019.

Supplementary Information

S1. Data Access and Reproducibility

All our continuum mechanical simulations of dynein were performed using FFEA, a software package in development at the University of Leeds. This software is available for download from the Bitbucket repository https://bitbucket.org/FFEA/ffea/src/master/. Although the core software is in active development for additional applications and features, for reproducibility purposes the branch *CytoDyneinParam* will remain unchanged and can be used to reproduce the work

Electronic supplementary information (ESI) contains all data and graphs used in this work, as well as additional movies which show the PCA normal modes calculated in this work. The full dataset is available as a downloadable tarball, and movies are available for independent download[26].

S2. Residues used to Define Vectors

To calculate the angular fluctuations of the stalk and linker domains, we defined the two vectors $\vec{v}_s$ and $\vec{v}_l$:

$$\vec{v}_s = \vec{v}_{s,h} - \vec{v}_{s,b} \quad \text{(S1)}$$

$$\vec{v}_l = \vec{v}_{l,h} - \vec{v}_{l,b} \quad \text{(S2)}$$

where $\vec{v}_{s,h}$ and $\vec{v}_{s,b}$ are calculated at each simulation frame as the centroid of a set of residues at the head and the base of the stalk and linker domains. Table S1 details the set of residues for each vector.

	Domain	
Vector	Stalk	Linker
$\vec{v}_{D,b}$	3267-3271, 3589-3593	1787-1791, 1801-1805
$\vec{v}_{D,h}$	3354-3358, 3504-3508	1480-1486, 1514-1520

Table S1. Residues used to define the end-to-end structural vectors for both the ADP and ATP atomistic models, and used to calculate angular fluctuations.

To calculate the contour length fluctuations of the stalk and linker domains, we subdivided the vectors $\vec{v}_s$ and $\vec{v}_l$ into vectors $\vec{v}_{s,i}$ and $\vec{v}_{l,i}$, such that:

$$\vec{v}_s = \sum_{i=0}^{N_s} \vec{v}_{s,i+1} - \vec{v}_{s,i} \quad \text{(S3)}$$

$$\vec{v}_l = \sum_{i=0}^{N_l} \vec{v}_{l,i+1} - \vec{v}_{l,i} \qquad \text{(S4)}$$

These residues are detailed in Table S2.

	Domain	
Vector	Stalk	Linker
$\vec{v}_{D,0}$	3267-3271, 3589-3593	1787-1791, 1801-1805
$\vec{v}_{D,1}$	3275-3279, 3580-3584	1624-1628, 1692, 1765
$\vec{v}_{D,2}$	3284-3288, 3572-3576	1648-1652, 1602, 1668
$\vec{v}_{D,3}$	3293-3297, 3563-3567	1530-1534, 1587-1591
$\vec{v}_{D,4}$	3301-3305, 3555-3559	1480-1486, 1514-1520
$\vec{v}_{D,5}$	3310-3314, 3546-3550	
$\vec{v}_{D,6}$	3319-3323, 3538-3542	
$\vec{v}_{D,7}$	3327-3331, 3529-3533	
$\vec{v}_{D,8}$	3336-3340, 3521-3525	
$\vec{v}_{D,9}$	3345-3349, 3512-3516	
$\vec{v}_{D,10}$	3354-3358, 3504-3508	

Table S2. Residues used to define the contour structural vectors for both the ADP and ATP atomistic models, and used to calculate contour length fluctuations. Note that the initial and final sets of residues in each domain are equivalent to those in Table S1.

S3. Assessment of Statistical Convergence of Molecular Dynamics Simulations

To determine whether the convergence behaviour of our MD simulations, we calculated the time evolution of the variance of each of the fluctuating parameters of the molecule. This data is shown in Figure S1.

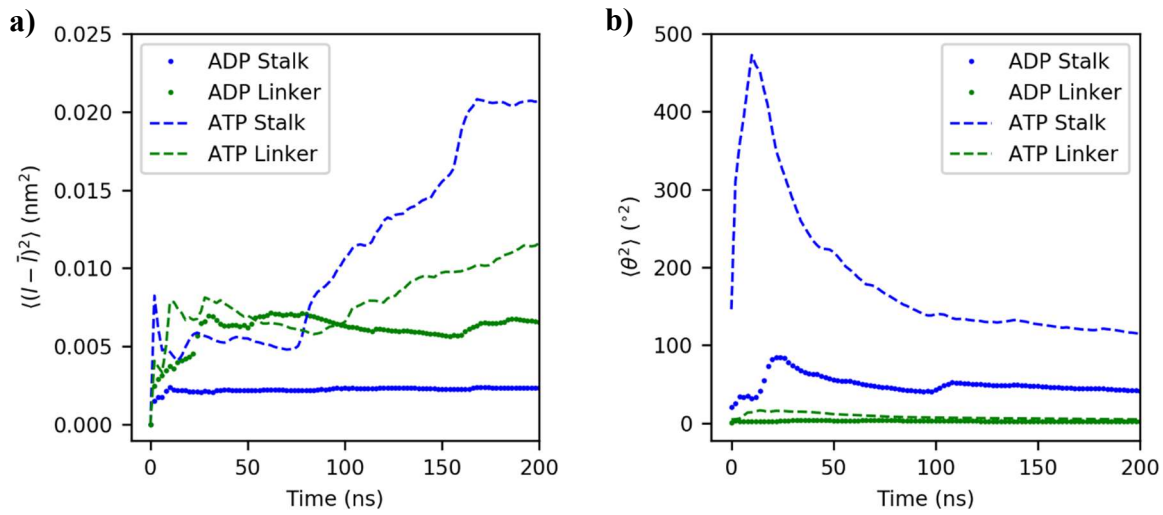

Figure S1. The evolution of the variance of each parameter over the course of the simulation, where **a)** corresponds to the contour length distributions, and **b)** to the angular distributions.

We can see that over the 200ns simulation, the angular fluctuations appear to be converging continuously towards an asymptotic variance, implying ergodicity in these parameters for both models. However, for the contour fluctuations shown in Figure 7a, whilst the ADP model appears relatively well converged, it is unclear as to whether the ATP model simulations are close to convergence or not. Combined with the bimodal Gaussian distribution shown in Figure 4b, we see that it would be inappropriate to parameterise our subsequent FFEA simulations using these contour fluctuation variances without additional MD simulation time. It is appropriate, as stated in the main text and given these traces, to take the angular fluctuations forward in our parameterisation regime. Note that the angular fluctuations make a far more significant contribution to the dynamics.